EFDA–JET–CP(09)01/04

D. Alves, R. Coelho, A. Klein, T. Panis, A. Murari
and JET EFDA contributors

A Real-Time Synchronous Detector for the TAE Antenna Diagnostic at JET

A Real-Time Synchronous Detector for the TAE Antenna Diagnostic at JET

D. Alves, R. Coelho, A. Klein, T. Panis, A. Murari
and JET EFDA contributors*

JET-EFDA, Culham Science Centre, OX14 3DB, Abingdon, UK

[1]Associação EURATOM/IST, Instituto de Plasmas e Fusão Nuclear, Av. Rovisco Pais 1049-001, Lisboa, Portugal
[2]MIT Plasma Science and Fusion Center, Cambridge, MA 02139, USA.
[3]CRPP, Association EURATOM – Confédération Suisse, EPFL, Lausanne, Switzerland.
[4]Consorzio RFX-Associazione EURATOM-ENEA per la Fusione. l-35127 Padua, Italy.
** See annex of F. Romanelli et al, "Overview of JET Results",*
(Proc. 22 [nd] IAEA Fusion Energy Conference, Geneva, Switzerland (2008)).

Preprint of Paper to be submitted for publication in Proceedings of the
16th IEEE NPSS Real Time Conference, Beijing, China.
(10th May 2009 - 15th May 2009)

ABSTRACT.
Routine studies are performed on JET using a new set of antennas to excite Toroidal Alfven Eigenmodes (TAE). A TAE resonances footprint is observed in the plasma response measurement when there is a noticeable variation in both the amplitude and the phase of the response with respect to the excitation. An algorithm for real-time identification of TAE resonances, based on a hardware lock-in amplifier, is presently used at JET for detecting such variations. In the paper, we revisit the problem of estimating the I-Q characteristics from a known non-stationary frequency mode, with a resonant-like phase response, embedded in a digital signal. A non-stationary linear model is used in a recursive filter implementation of a lock-in amplifier. We propose it as a viable alternative to hardware synchronous detectors such as the one in use at JET and compare its' performance with standard digital lock-in techniques in terms of bandwidth and phase response under high throughput rates requirements.

1. INTRODUCTION

he usefulness of MagnetoHydroDynamic (MHD) spectroscopy markers in the characterization of tokamak plasmas is widely recognized since it adds valuable information on the already broad span of measurements from plasma diagnostics. One particular useful marker targets a particular type of plasma instabilities identified as Toroidal Alfvén Eigenmode (TAEs) [1]. The resonant wave-particle interaction between these modes and the fusion born alpha particles (He4 ions) may lead both to the destabilization of the modes [2] and to the stochastization of the alpha particles orbit, with a consequent particle and energy confinement loss and possible damage to the first wall [3]. Assessing the damping/growth rates, frequency and wavenumber analysis of TAEs may therefore provide valuable information on bulk plasma stability and fast particle confinement losses. The conventional approach to carry out the former is to drive the modes with dedicated antennas [4,5], operating at frequencies within the range where TAEs are expected to propagate, according to some theoretical model. When the antenna resonates with a particular TAE eigenmode in the plasma, there is a significant increase in the plasma response that is clearly observed in the measured signals of relevant diagnostics (e.g. magnetic Mirnov probes, soft X-ray tomography, microwave reflectometry or beam emission spectroscopy [6]) by noticeable variations in both the amplitude and the phase shift with respect to the excitation. In order to measure the amplitude and the phase of selected signal components immersed in noise and compare to the excitation signal, lock-in amplifiers or synchronous detectors are beyond any doubt the natural solution. This inherently Fourier based method is widely used as a precision electronics measurement tool that plays a fundamental role not only in experimental physics, but also in modern science and engineering in general [7-9]. In this work, a general overview of the possible implementations of synchronous detection systems for the analysis of the transfer function of resonant excitation of TAEs is addressed. Focusing in more detail on the real-time techniques for estimating the amplitude and phase of the plasma response, a Kalman Filtering (KF) [10] digital signal processing approach is investigated as a promising

candidate to provide very high throughput estimates with flexible noise mitigation capabilities, capable of contrasting the more conventional Low-Pass Filtering (LPF) approaches that are native in a lock-in amplifier either digital or analog implementations. This work is therefore organized as follows : in the next Section a brief outline of the TAE antenna hardware presently used at JET is made together with a description of a characteristic TAE probing experiment, stimulating the need for synchronous detection schemes. In Section III, the principles of synchronous detection algorithms are overviewed, focusing on the merits and drawbacks of the hardware (analog) and software (digital) implementations that may come along in view of real-time processing. Section IV is dedicated to explain the fundamentals of a Kalman filtering implementation of a synchronous detection algorithm that allows for the estimation of the amplitude/phase of embedded quasi-periodic signals with tunable noise mitigation and sampling output. Concentrating on the particular case of TAE resonance excitation, two strategies are proposed for estimating the damping rate for modes with negligible driving sources, depending on whether one may dispose or not of the reference waveform driving the antennas. A novel implementation using the extended Kalman filter is shown where the amplitude of the plasma response is still recovered although no information is known about the exciting signal.

2. TAE ANTENNA DIAGNOSTIC

The JET tokamak was among the groundbreakers in actively exploring the TAE mode characteristics in hot relevant plasmas [4]. Early mode excitation employed the existing set of installed saddle coils that were more routinely used for error field correction. Due to the coil set up configuration, 4 coils separated 90^{o} toroidally in both lower and upper part of the torus ($75m^2$ in total), little flexibility could be achieved in the range of toroidal wavenumbers (labeled $\boldsymbol{n}$) that could be driven, i.e. $\boldsymbol{n}$ was limited to $|n| \leq 2$ depending on the phasing (positive/negative) of each coil. However, probing the full range of foreseen Alfven Eigenmodes (AE) modes for JET was possible owing to a broadband power amplifier of 3kW with a frequency span between ~30kHz up to 500kHz. The peak current and voltage induced in the saddle coils were, respectively, 30A and 500V. The driven magnetic field in the plasma core didn't perturb the plasma significantly owing to a low normalized $\delta B / B < 10^{-5}$ where δB represents the magnitude of the induced magnetic field perturbation and B a typical value for the toroidal field (~1-3T). After 2005, an upgrade to the diagnostic was carried out [11] to allow for a much more compact setup and consequently higher toroidal mode probing. Two sets of 4 rectangular coils toroidally apart were installed, each made of 18 loops with 25 × 25cm covering a total area of $\sim 0.5m^2$ in total and placed 4cm behind the poloidal limiter. This results on a wider range of toroidal modes that can be excited ($|n| \leq 50$). An upgrade to the broadband amplifier to 5kW was made and current and voltage peak values of 15A and 700V are achieved, yielding a maximum magnetic perturbation in the range $\delta B \sim 10^{-9} - 10^{-8}$ (T).

Routine studies are performed on JET using this new set of TAE antennas to excite modes typically in the 100-400kHz frequency range and measure the plasma response with Mirnov coil

signals [12,13]. This identification mechanism is part of a closed feedback loop that controls the antennas' sweeping frequency direction in order to maximize the number of resonant crossings during a JET pulse. The frequency of the driving magnetic perturbations is controlled by a Voltage Controlled Oscillator (VCO) with characteristic sweeping values of 200kHz/s setting the time and frequency resolution of the measurements for the damping rate and resonant frequency. This is shown in Figure 1 for JET Pulse No: 69571 where the resonance matching is clearly evidenced in the spectrogram from a Mirnov signal.

The spectrogram, however, provides only a first insight of where the resonance lies in frequency space but not on the actual damping rate of the mode being driven. A practical estimate, adequate for a real-time implementation, for the damping rate may be derived from the Full Width at Half Maximum (FWHM) of the measured amplitude response as a function of the probing frequency and the resonant frequency is simply obtained from the maximum response. Alternatively, more refined measurements are possible from the transfer function $H(\omega) = M(\omega)/R(\omega)$, where M and R stand, respectively, for the complex valued plasma response and the reference excitation. Resonances manifest themselves as poles in the transfer function, from which one extract the damping and frequency from the real and imaginary components.

Synchronous detection basically attempts to identify the components of the plasma response, with the same frequency as the excitation, that are in-phase and in quadrature (I-Q) with the excitation. In a complex plane representation, I and Q represent the real and imaginary components of the response. Far away from the resonance, I and Q should remain constant thus indicating no change in both amplitude and phase while crossing the resonance eventually leads to a circular pattern in the complex plane.

At JET, the real-time identification of TAE resonances is based on a hardware INCAA based synchronous detection system with up to 48 channel boards. The I-Q components are obtained by analog mixing of the measured signal with inphase and quadrature references and applying an analog LowPass Filtering (LPF) with ~100Hz bandwidth. Although a hardware implementation for the synchronous detection is relatively straightforward, a software approach, in principle more flexible, less expensive and requiring less maintenance, is less trivially implemented. This will be examined in the next Section.

3. STANDARD METHODS FOR SYNCHRONOUS DETECTION

As illustrated in the previous section, the quality of the TAE antenna diagnostic measurement is critically dependent on the effectiveness of the synchronous detection block. The goal is to estimate the amplitude and phase response of a system that exhibits a resonant behavior when subject to a known external excitation under certain conditions. The current hardware implementation of the synchronous detection can be equivalently done in software by means of a Fourier projection of the plasma response (Mirnov pick-up coil signal M) on to a unitary amplitude reference (R_{cos}) and quadrature (R_{sin}) signals components. Incidentally, the synchronous detection procedure just described

provides the basic principle of a Dual-Phase Lock-in (DPL) amplifier. In fact, in a DPL, both the amplitude (A) and relative phase difference (ϕ) of a given signal can be calculated quite easily, respectively, from $A = \sqrt{I^2 + Q^2}$ where one defines $I = \langle M(t)R_{\cos}(t)\rangle_{LPF}$ and $Q = \langle M(t)R_{\sin}(t)\rangle_{LPF}$ and $\phi = \tan^{-1}[Q/I]$. Alternatively, a less biased estimate of the amplitude may be obtained by mixing and low-pass filtering with a delayed reference that is in-phase with signal M(t).

This homodyne-type detection requires a large enough amount of samples to be used for the LPF to effectively filter out noise and provide the in-phase and quadrature components. These synchronous detectors are powerful methods although one may note some inherent shortcomings: noise mitigation may require large (order 100) of samples in a LPF Finite Impulse Response (FIR) implementation, thereby putting some pressure on the "processing burden" and inevitably introducing a time delay in the estimated amplitude and phase; it is best suited when there are no restrictions on the amount of samples used for the LPF-FIR; real-time tuning of the filter parameters for interplaying the low-pass region and the delay, although possible, is inherently an intricated problem since it requires the change in real-time, not only of the value of the filter coefficients, but also of their amount. Alternatively, one may opt for Infinite Impulse Response (IIR) filters. The performance of both types of filters is similar when compared the magnitude response characteristics with the delay introduced. Although IIR filters require a great deal less coefficients than the FIR filters for similar magnitude and phase responses, a particular attractive feature for real-time implementations, this comes at the price of, unlike the FIR filters, having a non-linear phase response. This, in practice, means that the IIR filters introduce different delays depending on the frequency components present in the signal and lead to distortions in the estimated signals. In the next section, an alternate algorithm for the synchronous detection problem using the Kalman filter is discussed and its advantages for a real-time implementation displayed.

4. THE KALMAN FILTER SYNCHRONOUS DETECTOR

The well established merits of the KF rely on its' state variable estimation scheme. The KF is the optimal quadratic estimator in linear systems corrupted with Gaussian distributed noise. It is fundamentally a predictor-corrector recursive estimator providing its' output based solely on the theoretical system model, the previous state estimation, its' current available measurement and on the balance between the model and measurement variances [10]. The KFs' performance, assuming the theoretical model is adequate for the problem at hand, is solely controlled by the ratio of the model and measurement variances. Ultimately, and assuming that, as usual, the measurement variance is an intrinsic characteristic of the measurement instrument, the KF can be tuned simply by changing the degree of confidence that is attributed to the model. Clearly, the KF assumes that both the measurement and system noise are non-correlated, zero mean and normally distributed random variables.

A harmonic estimator implementation of the KF [14,15] is intrinsically a time domain signal component estimator that provides, in a least square sense, both in-phase and quadrature projections of the signal over a time varying frequency path, thus suiting very well the purpose of implementing

a synchronous detector. The fundamental element in a Kalman filter modeling is the actual linear process matrix that describes how one passes from one time sample to the next with no knowledge of the actual measurement (the predictor step), i.e.

$$F(t) = \begin{bmatrix} cos(\Delta\theta(t)) & -sin(\Delta\theta(t)) \\ sin(\Delta\theta(t)) & cos(\Delta\theta(t)) \end{bmatrix} \tag{1}$$

where one is picturing that, in a complex plane representation, a quasi-periodic signal basically rotates by $\Delta\theta(t) = 2\pi f(t)/F$ at every time step while keeping the same amplitude (F_s is the sampling frequency). The predictor step that provides an *a priori* estimate for the state vector is given by

$$\hat{x}_k^- = F\hat{x}_{k-1} \tag{2}$$

where $\hat{x}_{k-1}$ is the estimated system state at sample *k-1*. The state vector in this case is a column matrix whose lines are the **in-phase** and **quadrature** signal components. A relation for the *a priori* error (difference between actual and estimated state variables) covariance is obtained as follows

$$P_k^- = FP_{k-1}F^T + Q \tag{3}$$

where Q is the covariance matrix for the theoretical model, i.e. it provides some measure of the inadequacy of the linear model to actually describe the process. The update (corrector) equation is given by

$$\hat{x}_k = \hat{x}_k^- + K_k(z_k - H\hat{x}_k^- \tag{4}$$

where the innovation is just a gain (K) multiplied by the residue, where an *a priori* measurement $H\hat{x}^-$ " is assumed. In this equation the gain, K_k, is given by

$$K_k = P_k^- H^T (HP_k^- H^T + R)^{-1} \tag{5}$$

where R is the measurement variance (a scalar). To close the system, the a-posteriori covariance is given by

$$P_k = (I - K_k H) P_k^- \tag{6}$$

Analyzing (4) and (5) leads immediately to two extreme and opposite limits of operation. When the uncertainty of the measurement tends to zero ($R \sim 0$) the KF estimation is simply the experimentally

derived system state. On the other hand, a big uncertainty in the measurement or, equivalently, a vanishing model uncertainty leads to a very small filter gain thus essentially disregarding the measurement.

An obvious and straightforward generalization is possible via block diagonally expanding the process matrix. This enables the KF harmonic estimator to simultaneously keep track of several periodic signals with different frequencies at runtime. In fact, the estimation quality of the signal component for a given frequency depends directly on the simultaneous estimation of all dominant frequency components [15].

In this particular case, we have the knowledge, at all times, of the frequency that we are requesting the VCO to produce but might or might not have the actual reference (excitation) signal fed to the antennas. As previously mentioned, resonance crossings can be identified by noticeable and characteristic changes in both the amplitude and relative phase difference in the Mirnov signal. In particular, one of the quantities of interest is the excited modes' damping rate. For this purpose one can either use the phase response, the amplitude response or both complementary. Clearly, extracting the instantaneous amplitude of the signal component of interest is a straightforward task (the amplitude at time sample k is just $A_k = \sqrt{\hat{x}_{2k-1}^2 + \hat{x}_{2k}^2}$, requires absolutely no knowledge of the reference signal and by analyzing the FWHM of the resonant peak one can also estimate the damping rate. If however one requires the phase difference estimation as a cross check, then it is critical to also acquire the in-phase and (estimate) the quadrature components of the reference signal, i.e. $\hat{x}_{ref,2k}$ and $\hat{x}_{ref,2k+1}$ respectively. Provided these are given, one can immediately build I~$sin(\phi)$, Q~$cos(\phi)$ as indicated in Section III and extract their phase difference (ϕ). If one is only given the reference signal itself, along with knowledge of the frequency requested to the VCO, one can build the quadrature component by using the KF estimator directly on the reference signal. This is a good advantage of the Kalman filter approach since it contributes to the overall simplification of the estimation process.

The present setup of the TAE antenna diagnostic in JET does not perform the acquisition of the VCO output signal which is essentially the excitation waveform that drives the antennas. Therefore, in order to perform a fair comparison between the DPL and the KF, the excitation and the plasma response signals have been synthesized with an amplitude and phase evolution as displayed, respectively, in Figures 2 and 3 and indicated by the black line. The input frequency of the excitation is swept with a trend similar to experiments and is indicated by the red line in Figure 6. The sampling frequency was set to 10^6 samples/s and normally distributed random noise yielding 0.5 signal-to-noise ratio was added to the synthetic Mirnov signal. As shown in Figures 2 and 3, the performance of the KF harmonic estimator for $RI/Q = 2\times10^4$ (where I is the 2×2 identity matrix) is comparable with the performance of the DPL with a FIR-LPF with 3kHz cutoff frequency and 400 taps (200 samples delay). Amplitude and phase estimations are provided in this case at a rate of 20×10^3 samples/s. It is worth mentioning that although a IIR-LPF would require less filter coefficients, its' non-linear phase response can introduce non-trivial and not acceptable signal distortion.

In many real-time systems running at a pre-defined cycle timing interval ($1/F_{out}$) a single estimation is often required to be derived entirely from the N samples acquired within the cycle itself ($N = F_s/F_{out}$ where F_s and F_{out} are, respectively, the sampling frequency and real-time network throughput rate). For the particular case where a 50kHz cycle time is required implying that only 20 samples are available each cycle, Figure 4 shows the comparison between the KF harmonic estimator and a DPL with a 20 tap (10 sample delay) FIR-LPF. The DPL obviously has a lower delay than the KF at the expense of noisier estimates. Also, whereas in the case of the DPL a change in the bandwidth/delay requires recalculation of the filter coefficients making it hard for performing online multirate signal processing, in the case of the KF harmonic estimator the only requirement is to change the RI/Q factor since the filter relies only on the previous system state estimation.

Clearly, the KF harmonic estimator provides relevant improvements over the DPL mainly in the cases when a predefined and fast cycle time imposes the usage of only a few samples for the LPF although its' robustness and ease of use make it essentially a more maintainable and updatable user friendly tool.

5. THE EXTENDED KALMAN FILTER FREQUENCY TRACKER

In the case when the amplitude estimation suffices for the calculation of both the resonant frequency (corresponding to peak in amplitude) and the damping rate (given by the FWHM), the reference waveform need not be known because it is only relevant for calculating the systems' phase response with respect to the excitation. The Extended Kalman Filter (EKF) [16, 17] Frequency Tracker (FT) [18,19] which is a non-linear application of the KF to the problem of frequency estimation is also a tool tailored to estimate both the frequency content of a signal and its' temporal evolution.

The intrinsic limitation of the KFs' linear model is clearly an obstacle when we acknowledge the overwhelming majority of real lifes' non-linear applications. In the EKF, the system state distribution is approximated by a gaussian random variable which is then propagated through the (first order) linear approximation of the non-linear model. This procedure has been extensively and successfully applied to non-linear estimation in the areas of state-estimation and machinelearning [20].

The single frequency matrix model for the EKF-FT given by (7) is merely an extension of (1).

$$F(t) = \begin{bmatrix} cos(\hat{x}_{3,k-1}) & -sin(\hat{x}_{3,k-1}) & 0 \\ sin(\hat{x}_{3,k-1}) & cos(\hat{x}_{3,k-1}) & 0 \\ 0 & 0 & 1-\varepsilon \end{bmatrix} \tag{7}$$

where $x = (x_1, x_2, x_3)^T$ and $\hat{x}_{3,k-1} = 2\pi f(t)/F_s$. The linearization of the model propagates to the estimation of the error covariance since the later is now given by

$$P_k^- = \Gamma P_{k-1} \Gamma^T + Q \tag{8}$$

where the Jacobian matrix $\Gamma = \frac{\partial [F\hat{x}_k^-]}{\partial x}$ is used. The filter gain is quite similar although the generalization encompasses also transfer matrices H that need not be constant, i.e.

$$K_k = P_k^- \, \Omega^T (\Omega P_k^- \, \Omega^T + R)^{-1} \tag{9}$$

$$\Omega = \frac{\partial H}{\partial x} \tag{10}$$

with the partial derivative denoting a Jacobian of the matrix.

The update of the state variable remains given by (4) where it was seen that the correction of the prediction is given as a function of the error term with a gain that is now provided by (9). The EKF is no longer the optimal linear quadratic estimator as it relies on (equivalently) a first order Taylor series approximation of the system model. It can also be shown that the EKF-FT provides an unbiased estimation of the unknown frequency only for $\varepsilon = 0$ [19]. Intuitively, it implies that from one time step to the next we are assuming in the model that the frequency doesn't change. Obviously this assumption, if not accurate, is amended in the corrector step of the algorithm and the estimated frequency is updated accordingly.

In Figure 5, the amplitude estimation performance comparison between the KF harmonic estimator and the EKFFT is shown. While the KF harmonic estimator requires the online knowledge of the signal frequency but does not require a reference signal, the EKF-FT not only needs none of that information but also provides its own estimation of the signal frequency (see Figure 6) with a similar signal-to-noise ratio and time delay.

CONCLUSION

In this work, an alternative strategy and implementation for the real-time synchronous detection of the plasma response to the excitation by the TAE antenna at JET was investigated. The Kalman filtering implementation of a lock-in amplifier was derived and shown that it is natively suitable for real-time data streams and consumes little resources when compared to the FIR/IIR LPFs required by conventional approaches. The Kalman filtering approach is also very flexible and low maintenance since it basically requires only the online tuning of the ratio between the measurements error covariance and the uncertainty in the underlying model that is considered to describe the measurements. In addition, and Extended Kalman Filtering implementation of a lock-in amplifier was shown to require absolutely no knowledge about the excitation waveform and, if one can use solely the amplitude of the plasma response to extract the required information, is a powerful method providing adaptively, as a parallel product, a high quality frequency estimation.

ACKNOWLEDGMENT

This work, supported by the European Communities and "Instituto Superior Técnico", has been carried out within the Contract of Association between EURATOM and IST. Financial support was

also received from “Fundação para a Ciência e Tecnologia” in the frame of the Contract of Associated Laboratory. The authors thank Dr. J. Sousa and Dr. B. Carvalho for enlightening comments.

REFERENCES

[1]. Cheng C.Z, et al., Ann. Phys., NY 161, 21 (1985)
[2]. Fu G.Y, . Van Dam J.W, Phys. Fluids B **1**, 1949 (1989)
[3]. Fasoli A., et al, Nucl. Fusion, **35**, 1485 (1995)
[4]. Fasoli A., et al, Phys. Rev. Lett. **75**, 645, (1995)
[5]. Snipes J.A., et al, Plasma Phys. Control. Fusion **46,** 611 (2004)
[6]. King-Lap Wong, Plasma Phys. Control. Fusion **41**, R1 (1999)
[7]. Mandelis A., Rev. Sci. Instrum. **65**, 3309 (1994)
[8]. Douglas C. Noll, Dwight G. Nishimura, IEEE Trans. on Med Imag., **IO**, 154, (1991)
[9]. Womack K.H., Opt. Engineering **23**, 391, (1984)
[10]. Kalman R.E, Transactions of the ASME–Journal of Basic Engineering **82** (Series D): 35-45 (1960)
[11]. Testa D., et al., 23rd Symposium on Fusion Technology (SOFT), Venice (Italy), 20-24 September 2004
[12]. Testa D., et al, Proc. 34th EPS Conference on Plasma Phys. Warsaw, 2 - 6 July 2007 ECA Vol.**31F**, P-5.068 (2007)
[13]. Klein A., et al, Proc. 35th EPS Conference on Plasma Phys. Hersonissos, 9 - 13 June 2008 ECA Vol.**32D**, P-5.083 (2008)
[14]. Caciotta M., P. Carbone, Instrumentation and Measurement Technology Conference, 1996. IMTC-96. Conference Proceedings. ‘Quality Measurements: The Indispensable Bridge between Theory and Reality’., IEEE **1**, 470 (1996)
[15]. Coelho R., Alves D., IEEE Trans. on Plasma Science, **37**,164 (2009)
[16]. Jazwinski A.H., Stochastic Processes and Filtering Theory. San Diego, CA: Academic, 1970.
[17]. Sorenson H.W., Ed., Kalman Filtering: Theory and Application Piscataway, NJ: IEEE, 1985.
[18]. La Scala B.F., Bitmead R.R, IEEE Transactions on Signal Processing **44**, 739 (1996)
[19]. Bittanti S., Savaresi S.M., IEEE Transactions on Automatic Control **45**, 1718 (2000)
[20]. Julier S.J. and Uhlmann J.K., A New Extension of the Kalman Filter to Nonlinear Systems. In The Proceedings of AeroSense: The 11th International Symposium on Aerospace/Defense Sensing, Simulation and Controls, Orlando, FL, USA, 1997. SPIE. Multi Sensor Fusion, Tracking and Resource Management II.

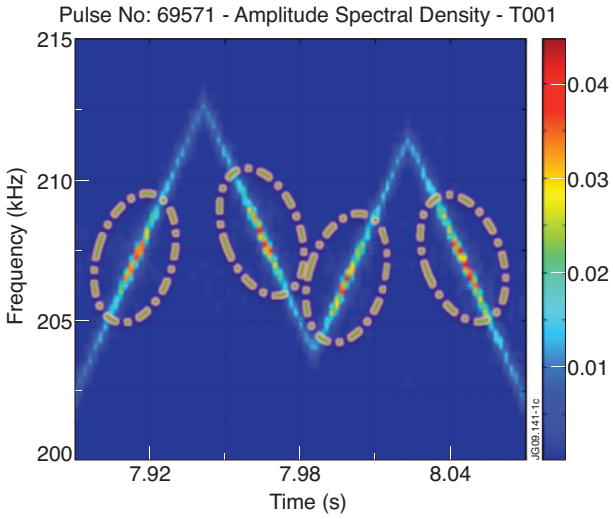

Figure 1: Typical spectrogram of a Mirnov coil signal showing clearly the frequency sweeps and resonant spots.

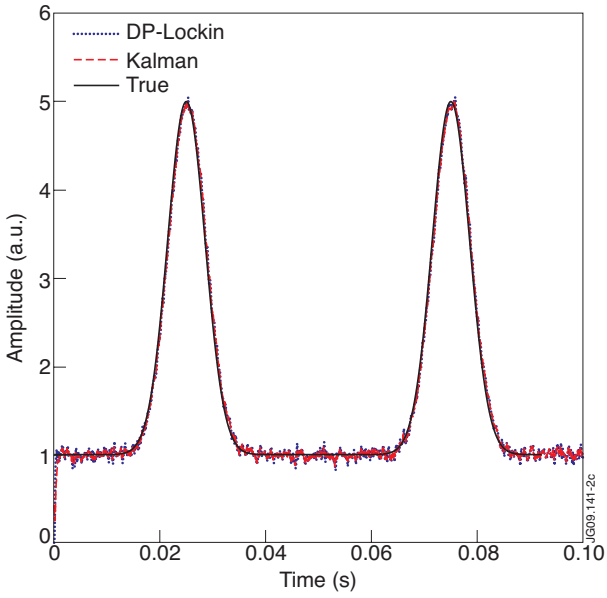

Figure 2: DPL and Kalman amplitude estimation

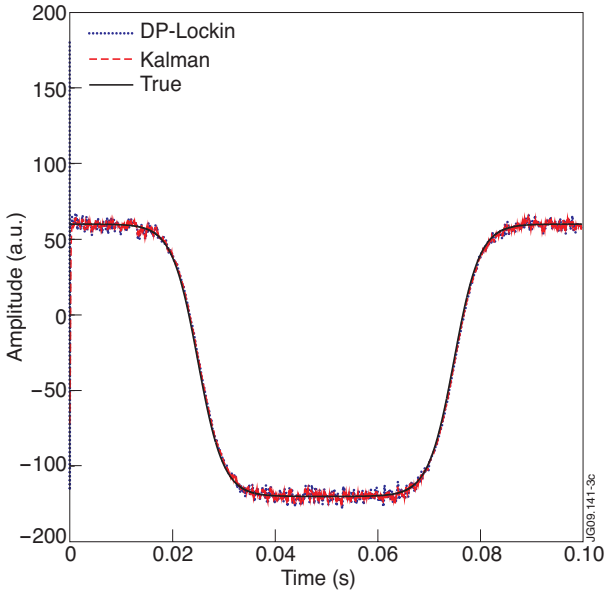

Figure 3: DP and Kalman phase estimation

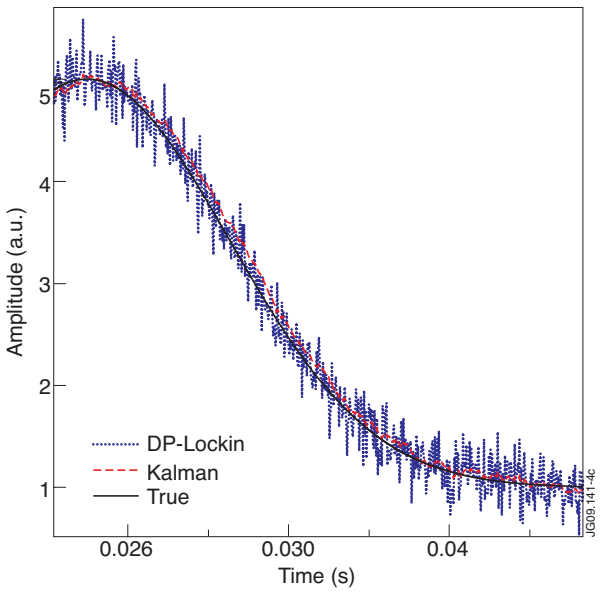

Figure 4: DPL and Kalman amplitude estimation

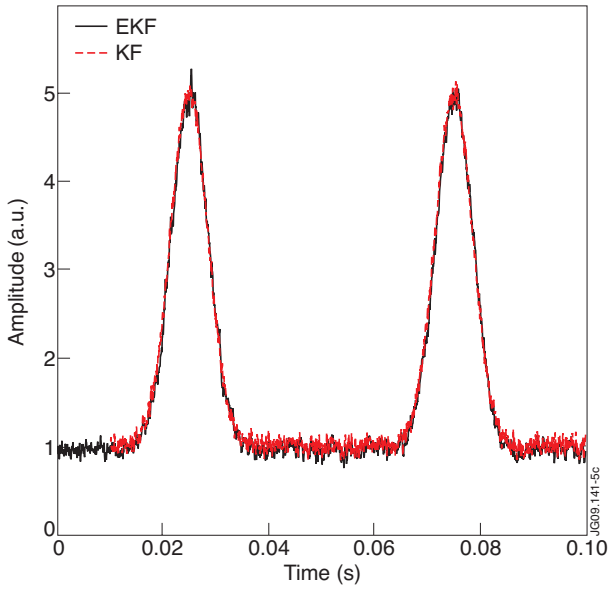

Figure 5: Amplitude estimation performance comparison between the KF and EKF.

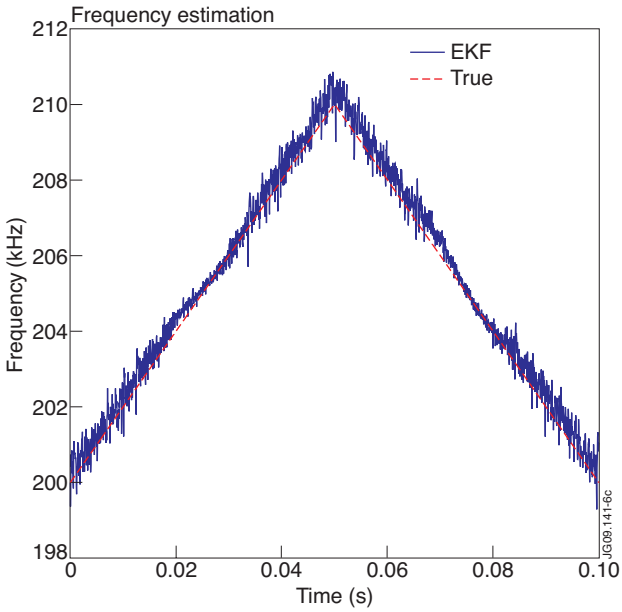

Figure 6: EKF frequency estimation.